

An Unusual Dresselhaus Spin-Orbit Contribution of Even Order in Momentum

Hao Yang,¹ Wei Wang,² Gerson J. Ferreira,³ Ning Hao,⁴ Ping Zhang,^{1,5} and Jiyong Fu^{1,*}

¹Department of Physics, Qufu Normal University, Qufu 273165, Shandong, China

²Department of Physics, Jining University, 273155 Qufu, Shandong, China

³Instituto de Física, Universidade Federal de Uberlândia, Uberlândia, Minas Gerais 38400-902, Brazil

⁴Anhui Province Key Laboratory of Low-Energy Quantum Materials and Devices,

High Magnetic Field Laboratory, HFIPS, Chinese Academy of Sciences, Hefei, Anhui 230031, China

⁵Beijing Computational Science Research Center, Beijing 100084, China

The spin-orbit (SO) coupling is conventionally known to manifest as *odd* functions of momentum. Here, through both model calculations and symmetry analysis along with the method of invariants, we reveal that, in ordinary semiconductor heterostructures, a *quadratic* Dresselhaus SO term— inheriting from its bulk crystal form—emerges via the interband effect, while complying with time-reversal and spatial symmetries. Furthermore, we observe that this unusual SO term gives rise to a range of striking quantum phenomena, including hybridized swirling texture, anisotropic energy dispersion, avoided band crossing, longitudinal *Zitterbewegung*, and opposite spin evolution between different bands in quantum dynamics. These stand in stark contrast to those associated with the usual *linear* SO terms. Our findings uncover a previously overlooked route for exploiting interband effects and open new avenues for spintronic functionalities that leverage unusual SO terms of *even* orders in momentum.

Introduction.— The spin-orbit (SO) interaction, which facilitates coherent spin manipulation, is a key ingredient in spintronic devices [1–8]. In semiconductor nanostructures, the SO effects usually have two dominant contributions: the Rashba [9] and Dresselhaus [10] terms, arising from the structural and crystal inversion asymmetries, respectively. Constrained by time-reversal symmetry (TRS), the SO coupling is conventionally expected to appear as *odd* functions of momentum. The Rashba term is *linear*, and can be tuned with the doping profile [11] as well as *in situ* using gate voltages [12, 13]. The Dresselhaus term inherits its bulk three-dimensional (3D) source but with a reduced two-dimensional (2D) form [14–16], which can be decomposed into both *linear* and *cubic* terms of odd orders in momentum [14–18].

Here, for two-dimensional electron gases (2DEGs) confined in ordinary semiconductor heterostructures [Fig. 1(a)], we demonstrate that the interband coupling enables the emergence of a *quadratic* [$\Gamma^{(2)}$; Fig. 1(b)] Dresselhaus SO term, while remaining fully consistent with TRS. This unusual SO term is supported by both our model calculations and symmetry analysis along with the method of invariants [19]. Furthermore, we observe that the unusual SO term induces diverse spin-related phenomena, including hybridized swirling texture, anisotropic energy dispersion, avoided band crossing [Fig. 2], longitudinal *Zitterbewegung*, and opposite spin evolution between different bands in quantum dynamics [Figs. 3 and 4]. All these stand in stark contrast to those associated with the usual *linear* SO term. Our work uncovers a previously overlooked facet of SO physics in nanostructures and points toward novel strategies for spintronic applications that leverage interband effect and unusual SO terms of *even* orders.

Model Hamiltonian.— We start from the bulk Dresselhaus cubic SO coupling in zincblende crystals [10],

$$\mathcal{H}_{\mathcal{D}}^{\text{bulk}} = (\gamma/\hbar)[\sigma_x p_x(p_y^2 - p_z^2) + \text{c.p.}], \quad (1)$$

with $p_{x,y,z}$ being the electron momentum components along

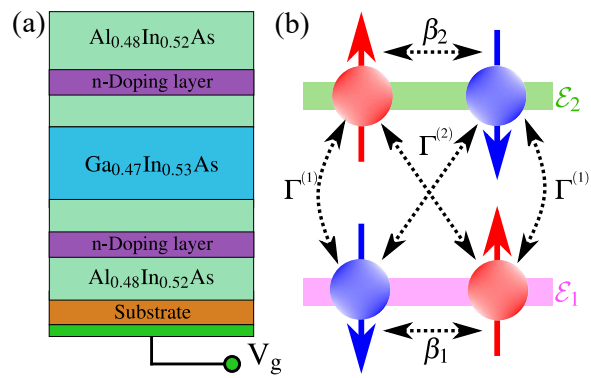


Figure 1. (Color online) (a) Growth profile of an *n*-doped $\text{Al}_{0.48}\text{In}_{0.52}\text{As}/\text{Ga}_{0.47}\text{In}_{0.53}\text{As}$ quantum well subject to gate voltage V_g , and the potential profile for 2DEGs with two-band energies ε_1 and ε_2 . (b) Illustration of intra- and interband Dresselhaus SO couplings with spin and band degrees of freedom. Here β_v ($v = 1, 2$) denotes the intraband SO connecting distinct spins within the same v -th band, and $\Gamma^{(1)}$ ($\Gamma^{(2)}$) represents the linear (quadratic) interband SO between spins of opposite (same) orientations. The red and blue arrows stand for the spin-up and spin-down states, respectively.

the $x \parallel [100]$, $y \parallel [010]$ and $z \parallel [001]$ directions, $\sigma_{x,y,z}$ referring to the Pauli matrices, and γ as the bulk Dresselhaus parameter.

We consider 2DEGs confined in semiconductor quantum wells grown along the z direction. Hence, we have the overall 3D Dresselhaus SO Hamiltonian,

$$H = H_0 + \mathcal{H}_{\mathcal{D}(1)}^{\text{3D}} + \mathcal{H}_{\mathcal{D}(2)}^{\text{3D}} + \mathcal{H}_{\mathcal{D}(3)}^{\text{3D}}, \quad (2)$$

in which $H_0 = \hbar^2(k_x^2 + k_y^2)/2m^* + k_z(\hbar^2/2m^*)k_z + V_{sc}(z)$, $m^* \equiv m^*(z)$ is the z -dependent effective electron mass and $k_z = -i\partial_z$. Here V_{sc} denotes the self-consistent potential felt by the confined 2DEGs. It comprises the structural part V_w , the electronic Hartree potential V_e , the doping potential V_d and an external gate V_g . The other terms in H , namely $\mathcal{H}_{\mathcal{D}(i)}^{\text{3D}}$, denote the i -th order Dresselhaus SO contribution, with $\mathcal{H}_{\mathcal{D}(1)}^{\text{3D}} =$

$k_z \gamma(z) k_z (\sigma_y k_y - \sigma_x k_x)$, $\mathcal{H}_{\mathcal{D}(2)}^{3D} = (1/2)(\gamma(z) k_z + k_z \gamma(z)) \sigma_z (k_x^2 - k_y^2)$, and $\mathcal{H}_{\mathcal{D}(3)}^{3D} = \gamma(z) k_x k_y (\sigma_x k_y - \sigma_y k_x)$. Note that here we have performed the usual *symmetrization* procedure [20] since $\gamma(z)$ and k_z do not commute.

We now derive an effective 2D Hamiltonian by projecting H [Eq. (2)] onto the *two* lowest spin-degenerate eigensolutions of H_0 : $\langle \mathbf{r}|\mathbf{k}, \nu, \sigma \rangle = e^{i\mathbf{k}\cdot\mathbf{r}} \varphi_\nu(z) |\sigma_z\rangle$, $\nu = \{1, 2\}$, $\sigma_z = \{\uparrow, \downarrow\}$, with energies $\varepsilon_{\nu, k} = \varepsilon_\nu + \hbar^2 k^2 / 2m_{2D}^*$, where $\mathbf{k} = (k_x, k_y)$ is the in-plane wave vector, ε_ν is the ν th (self-consistent) energy level, and m_{2D}^* denotes the effective 2D electron mass [21]. We find the effective 4×4 2D Hamiltonian [22],

$$\mathcal{H} = \left(\frac{\hbar^2 k^2}{2m_{2D}^*} + \varepsilon_+ \right) \mathbb{1} \otimes \mathbb{1} - \varepsilon_- \tau_z \otimes \mathbb{1} + \mathcal{H}_D, \quad (3)$$

in which $\mathbb{1}$ the 2×2 identity matrix, $\varepsilon_\pm = (\varepsilon_2 \pm \varepsilon_1)/2$, τ_j ($j = x, y, z$) the Pauli matrices in the subband subspace, and \mathcal{H}_D the two-band Dresselhaus SO Hamiltonian,

$$\begin{aligned} \mathcal{H}_D = & \frac{g^* \mu_B}{2} [\mathbb{1} \otimes \boldsymbol{\sigma} \cdot \mathbf{B}_+^D(\mathbf{k}) - \tau_z \otimes \boldsymbol{\sigma} \cdot \mathbf{B}_-^D(\mathbf{k}) \\ & + \tau_x \otimes \boldsymbol{\sigma} \cdot \mathbf{B}_{12}^{D(1)}(\mathbf{k}) - \tau_y \otimes \boldsymbol{\sigma} \cdot \mathbf{B}_{12}^{D(2)}(\mathbf{k})], \end{aligned} \quad (4)$$

where g^* is the effective g-factor, μ_B is the Bohr magneton, $\mathbf{B}_\pm^D = (\mathbf{B}_2^D \pm \mathbf{B}_1^D)/2$, and \mathbf{B}_ν^D is the *intraband* Dresselhaus field,

$$\mathbf{B}_\nu^D = \frac{2k\beta_\nu}{g^* \mu_B} (\sin \theta \hat{\mathbf{y}} - \cos \theta \hat{\mathbf{x}}), \quad (5)$$

with $\tan \theta = k_y/k_x$ and the intraband Dresselhaus strength $\beta_\nu = \langle v | \partial_z \gamma(z) \partial_z | v \rangle$ [Fig. 1(b)]. The linear ($\mathbf{B}_{12}^{D(1)}$) and quadratic ($\mathbf{B}_{12}^{D(2)}$) *interband* Dresselhaus fields read as

$$\begin{aligned} \mathbf{B}_{12}^{D(1)} &= \frac{2k\Gamma^{(1)}}{g^* \mu_B} (\sin \theta \hat{\mathbf{y}} - \cos \theta \hat{\mathbf{x}}), \\ \mathbf{B}_{12}^{D(2)} &= \frac{2k^2 \Gamma^{(2)}}{g^* \mu_B} \cos 2\theta \hat{\mathbf{z}}, \end{aligned} \quad (6)$$

with $\Gamma^{(1)} = \gamma(1| \partial_z \gamma(z) \partial_z | 2)$ [$\Gamma^{(2)} = -(1/2)(1| \gamma(z) \partial_z + \partial_z \gamma(z) | 2)$] as the linear [quadratic] SO coefficients [Fig. 1(b)].

Symmetry analysis and invariants method.— To corroborate our model, we further perform symmetry analysis [23] along with theory of invariants. Zincblende crystals belong to the space group $F\bar{4}3m$ [24], which comprises the T_d point group and nonsymmorphic space translations. For heterostructures grown along the z direction, the three-fold rotation $C_3^{[111]}$ inherent to T_d is broken, and then the point group is reduced to either D_{2d} or C_{2v} , depending on whether the system is symmetric or asymmetric. For a general case with asymmetric configuration, the relevant symmetry reduces to the point group C_{2v} along with time-reversal symmetry \mathcal{T} . Within the method of invariants [19], the effective 2D Hamiltonian $\mathcal{H}(\mathbf{k})$ must satisfy $\mathcal{H}(D^k(S)\mathbf{k}) = D^\psi(S)\mathcal{H}(\mathbf{k})D^{\psi-1}(S)$, for every symmetry operation $S \in C_{2v} \oplus \mathcal{T}$, where D^ψ stands for the representation of basis functions and D^k the representation acting on \mathbf{k} . With all these considerations, we obtain the results that are fully consistent with those from our model calculations, further supporting the existence of the quadratic SO term. For more details, including contributions from Rashba SO terms, see Sec. I of the supplementary material (SM).

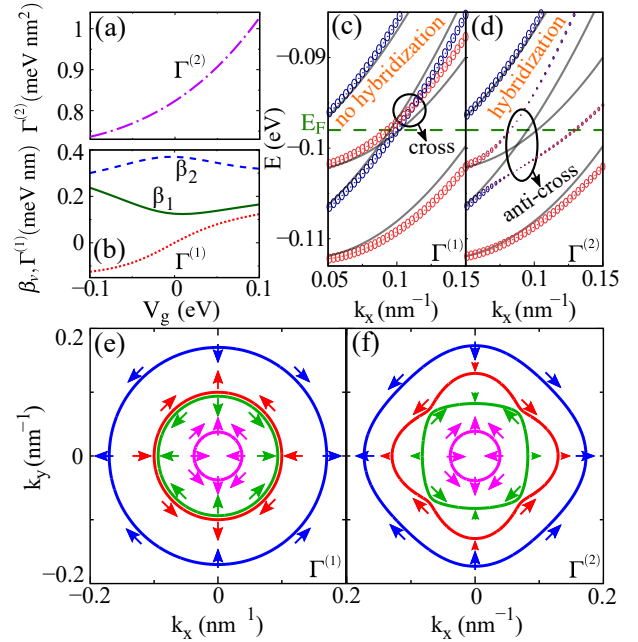


Figure 2. (Color online) (a) The quadratic (interband $\Gamma^{(2)}$) and (b) the linear (intraband β_ν and interband $\Gamma^{(1)}$) Dresselhaus SO coefficients versus V_g . (c), (d) Spin-resolved two-band energy dispersion (scaled by a factor of 100 for visibility) along the k_x direction, with interband coupling $\Gamma^{(1)}$ (c) and $\Gamma^{(2)}$ (d). The size of markers scales with the degree of spin polarization and the color represents spin orientations up (red) and down (blue). The gray (dashed) lines indicate the uncoupled ($\Gamma^{(1)} = \Gamma^{(2)} = 0$) bands. (e), (f) Constant-energy contours and spin textures at $E_F = -0.098$ eV [see horizontal (green) dashed line in (c) and (d)], for our system with $\Gamma^{(1)}$ (e) and $\Gamma^{(2)}$ (f).

System and self-consistent SO couplings.— We consider 2DEGs confined in n -doped $\text{Al}_{0.48}\text{In}_{0.52}\text{As}/\text{Ga}_{0.47}\text{In}_{0.53}\text{As}$ quantum well [Fig. 1(a)], similar to experimental samples of Ref. [25]. The well width is 45 nm, and a 6-nm wide doped region in the $\text{Al}_{0.48}\text{In}_{0.52}\text{As}$ layer is positioned 15 nm away from the well interface, with the doping density $\rho_d = 2.0 \times 10^{18} \text{ cm}^{-3}$. The effective electron masses are $m^* = 0.073m_0$ for $\text{Al}_{0.48}\text{In}_{0.52}\text{As}$ and $m^* = 0.043m_0$ for $\text{Ga}_{0.47}\text{In}_{0.53}\text{As}$ [26], respectively, with m_0 being the bare electron mass. To account for the mass discontinuity across different layers, we solve the Ben Daniel-Duke equation [20, 27] self-consistently with the Poisson equation, beyond using the usual Schrödinger equation. This yields eigensolutions used for obtaining the Dresselhaus terms of both intraband [Eq. (5)] and interband [Eq. (6)] types. At $V_g = 0.1$ eV, we obtain $\beta_1 = 0.16 \text{ meV nm}$, $\beta_2 = 0.32 \text{ meV nm}$, $\Gamma^{(1)} = 0.1 \text{ meV nm}$, and $\Gamma^{(2)} = 1.02 \text{ meV nm}^2$ [Figs. 2(a) and 2(b)], which are used to explore below the spin-related phenomena.

Anisotropic Fermi contours, swirling textures and spin hybridizations.— Figure 2(c) [2(d)] show spin-resolved dispersions as functions of k_x , illustrating the effects of the linear $\Gamma^{(1)}$ [quadratic $\Gamma^{(2)}$] interband SO term. For the quadratic term $\Gamma^{(2)}$ [Fig. 2(d)], a clear band anticrossing appears between the inner two spin branches, as compared to uncoupled (crossed)

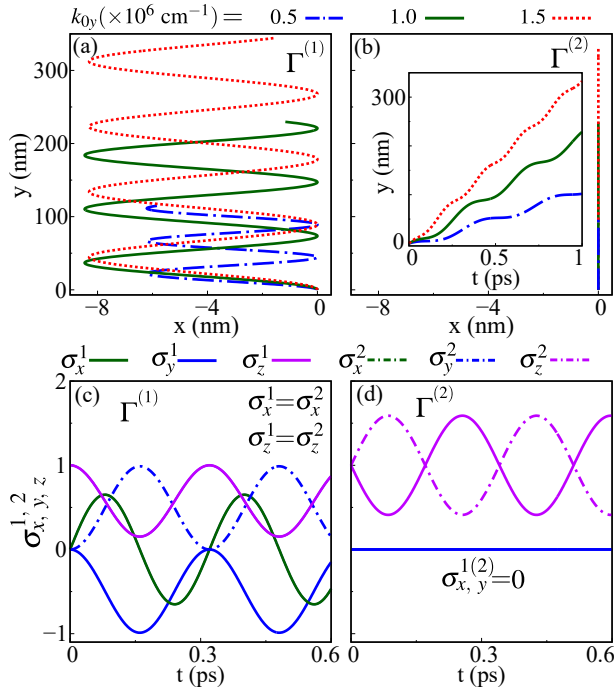


Figure 3. (Color online) (a), (b) *Zitterbewegung* induced by the linear ($\Gamma^{(1)}$) (a) and quadratic ($\Gamma^{(2)}$) (b) interband SO terms, for the *initial* (group) velocity $\mathbf{v}_g = \hbar k_{0y}/m^* \hat{\mathbf{y}}$ (along the y direction) with $k_{0y} = \{0.5, 1.0, 1.5\} \times 10^6 \text{ cm}^{-1}$. In (b), the x -direction motion vanishes for all k_{0y} ; the inset shows the y -direction trajectory over time. (c), (d) Time evolution of spin components $\sigma_{x,y,z}^v$ ($v = 1, 2$) for the two bands in the presence of $\Gamma^{(1)}$ (c) and $\Gamma^{(2)}$ (d), at $k_{0y} = 1.0 \times 10^6 \text{ cm}^{-1}$.

bands ($\Gamma^{(2)} = 0$) [gray lines in Fig. 2(d)]. This stems from that $\Gamma^{(2)}$ couples the same spin states across different bands [Fig. 1(b)]. Notably, near the anticrossing point, the spin polarization nearly vanishes, as reflected by diminishing size of the markers. This suppression of spin polarization arises from the *hybridization* of different spin branches. In sharp contrast, when only the linear term $\Gamma^{(1)}$ is present [Fig. 2(c)], we observe that (i) the band dispersions remain crossed, resembling the behavior of uncoupled bands [gray lines in Fig. 2(c)], and that (ii) no spin hybridization occurs. These distinct spin-resolved features have significant implications for spintronic functionalities, e.g., intrinsic spin-Hall effect [28] and efficient spin-charge interconversion [29, 30]. Note that the interband SO coupling has been experimentally verified in Bi-Ag-Au heterostructures with unusual spin textures [31].

In Fig. 2(f), we show the swirling spin texture traced along the constant-energy contours $E(\mathbf{k}) = E_F$ [green dashed horizontal line in Fig. 2(d)] in the k_x - k_y plane under the impact of quadratic term $\Gamma^{(2)}$. The arrows along the contours denote the spin vector field $\langle \boldsymbol{\sigma} \rangle$. Beyond inducing spin hybridization and band anticrossing, we find that the presence of $\Gamma^{(2)}$ also leads to pronounced anisotropy in the energy dispersion. Such anisotropy is expected to manifest in measurable transport properties, e.g., directional dependence in the charge conductivity tensor. And, this behavior stands contrast to the case

with only the linear term $\Gamma^{(1)}$, where both the energy dispersion and the spin texture remain isotropic [Fig. 2(e)].

Novel longitudinal Zitterbewegung.— The dynamics of electron wave packets with SO interaction exhibits an oscillatory (trembling) motion known as *Zitterbewegung* [32–36]. With the help of Ehrenfest’s theorem [37, 38], we have,

$$\frac{\partial \langle x \rangle}{\partial t} = \left\langle \frac{\partial \mathcal{H}_D}{\partial p_x} \right\rangle, \quad \frac{\partial \langle y \rangle}{\partial t} = \left\langle \frac{\partial \mathcal{H}_D}{\partial p_y} \right\rangle, \quad \frac{\partial \langle \zeta \rangle}{\partial t} = \frac{i}{\hbar} \langle [\mathcal{H}_D, \zeta] \rangle, \quad (7)$$

where ζ denotes the *pseudospin-spin* tensor that we define to account for the presence of interband coupling involving both spin (σ) and subband (τ ; pseudospin) degrees of freedom, $\zeta = \sum_{i,j} \zeta_{ij} \mathbf{i} \otimes \mathbf{j}$, with $\zeta_{ij} = \tau_i \otimes \sigma_j$. Here the indices $i, j = 0, 1, 2, 3$, with $\tau_0 = \sigma_0 = \mathbb{1}$ (identity matrix), and $\{\tau_{1,2,3}\}, \{\sigma_{1,2,3}\}$ the standard Pauli matrices acting in the subband and spin subspaces [Eq. (3)], respectively. For simplicity, yet without lack of generality, we determine the expectation value of position operator $\mathbf{r}(t) = \{x(t), y(t)\}$ with respect to plane waves (referring to ‘large’ wave packets). Initially, we consider spin-up electrons injected into both of the two bands along the y axis with group velocity $\mathbf{v}_g = \hbar k_{0y}/m^* \hat{\mathbf{y}}$, i.e., $\sigma_z^1(0) = \sigma_z^2(0) = 1$, and assume $x(0) = y(0) = 0$. For simplifying notations, in what follows we omit the $\langle \cdots \rangle$ notation, such that the position variables (x, y) and the pseudospin-spin operators (ζ_{ij}) [Eq. (7)] are to be interpreted as expectation values, i.e., $x \rightarrow \langle x \rangle, y \rightarrow \langle y \rangle, \zeta_{ij} \rightarrow \langle \zeta_{ij} \rangle$.

In order to fully capture the interband effect, we first ignore the intraband terms [$\beta_1 = \beta_2 = 0$; Eq. (5)]. Interestingly, based on Eqs. (4) and (7), we obtain compact expressions for spatial trajectories of electrons arising from both the linear ($\Gamma^{(1)}$) and quadratic ($\Gamma^{(2)}$) interband SO contributions [Eq. (6)]. In the purely linear case, we obtain,

$$x(t) = \frac{4k_{0y}\Gamma^{(1)2} [\cos(\Omega^{(1)}t) - 1]}{\hbar^2\Omega^{(1)2}}, \quad y(t) = \frac{\hbar k_{0y}t}{m^*}, \quad (8)$$

and for the purely quadratic case, we have,

$$x(t) = 0, \quad y(t) = \frac{\hbar k_{0y}t}{m^*} + \frac{4k_{0y}\Delta\Gamma^{(2)} [\cos(\Omega^{(2)}t) - 1]}{\hbar^2\Omega^{(1)2}}, \quad (9)$$

where we have defined $\Omega^{(1)} = \sqrt{\Delta^2 + 4k_{0y}^2\Gamma^{(1)2}/\hbar}$ and $\Omega^{(2)} = \sqrt{\Delta^2 + 4k_{0y}^4\Gamma^{(2)2}/\hbar}$, with $\Delta = 2\varepsilon_-$ [Eq. (3)]. From Eq. (8), we find that for the linear term, the *Zitterbewegung* motion is always perpendicular to the initial group velocity \mathbf{v}_g ($\propto k_{0y}$), referring to usual scenario of the so-called transverse *Zitterbewegung* [Fig. 3(a); Figs. S3(a) and S3(b) in the SM]. This behavior resembles the *Zitterbewegung* induced by the *single-band* Dresselhaus SO interaction (see the SM; Sec. II). Remarkably, for the quadratic term, we uncover an unconventional *Zitterbewegung* that occurs along the longitudinal (k_y) direction (aligned with \mathbf{v}_g), while the trajectory along the transverse (k_x) direction remains pinned at zero [Fig. 3(b)]. This intriguing trembling motion is attributed to the unique symmetry of quadratic SO field with $\tau_y \otimes \boldsymbol{\sigma} \cdot \mathbf{B}_{12}^{D(2)}(\mathbf{k})$ [Eq. (4)].

Opposite spin dynamics between different bands.— In Figs. 3(c) and 3(d), we show time evolution of the three spin components $\sigma_{x,y,z}^v$ for each band ($v = 1, 2$), under the influence of linear and quadratic interband SO couplings, respectively. In the presence of linear term $\Gamma^{(1)}$ [Fig. 3(c)], we observe symmetric (identical) spin evolution in both the x and z components across the two bands, namely $\sigma_x^1 = \sigma_x^2$ and $\sigma_z^1 = \sigma_z^2$. In contrast, the y components of the two-band electron spins evolve antisymmetrically with $\sigma_y^1 = -\sigma_y^2$. This behavior reflects the presence of an effective internal magnetic field induced by $\Gamma^{(1)}$, which acts in opposite directions on the two bands along the y direction, while preserving identical spin precession dynamics within the x - z plane.

In contrast, under the quadratic term $\Gamma^{(2)}$ [Fig. 3(d)], we find that both σ_x^v and σ_y^v remain pinned at their initial value—zero—for both bands. Remarkably, the z component of the electron spins for the two bands exhibit opposite time evolution. Specifically, σ_z^1 and σ_z^2 evolve in opposite trend relative to their initial spin polarization, implying a spin separation effect between the two bands induced by the quadratic coupling. Since $\sigma_{x,y}^1$ and $\sigma_{x,y}^2$ are locked at zero, the overall spins σ^v of the two bands essentially have opposite dynamics.

To gain deeper insight into spin dynamics under interband SO coupling, we decompose the spin evolution by factoring the *pseudospin-spin* tensor ς_{ij} . Specifically, we find that the combinations $(\varsigma_{01} \pm \varsigma_{31}) \rightarrow \sigma_x^{1(2)}$, $(\varsigma_{02} \pm \varsigma_{32}) \rightarrow \sigma_y^{1(2)}$, and $(\varsigma_{03} \pm \varsigma_{33}) \rightarrow \sigma_z^{1(2)}$. This decomposition enables us to derive closed-form analytical expressions of the three spin components $\sigma_{x,y,z}^v$ of two bands (see the SM; Sec. III), in the presence of either linear or quadratic interband SO term, justifying our numerical outcomes. Also, as expected, we reveal that the oscillation period of spin is the same as that for the *Zitterbewegung* in real space, cf. Eq. (S58) in the SM and Eq. (9).

Intertwined effect between linear and quadratic interband terms.— When both $\Gamma^{(1)}$ and $\Gamma^{(2)}$ are present, the resulting spin dynamics exhibit novel features that go beyond those arising from either term alone—a phenomenon we refer to as *intertwined* effect of the two interband SO contributions. For the in-plane spin components, the contrasting roles of the two types of couplings become particularly evident. While the quadratic term $\Gamma^{(2)}$ alone yields vanishing in-plane spin components and the linear term $\Gamma^{(1)}$ alone results in antisymmetric y component between the two bands, we reveal that the presence of both $\Gamma^{(1)}$ and $\Gamma^{(2)}$ breaks this antisymmetry in σ_y^v , as shown in Fig. 4(a). This behavior originates from distinct symmetries associated with the linear and quadratic interband SO fields [Eqs. (5) and (6)]. For the x component, although the evolution remains symmetric ($\sigma_x^1 = \sigma_x^2$) between the two bands, the dynamical profile is markedly different from that observed under $\Gamma^{(1)}$ only, cf. Figs. 4(a) and 3(c).

In addition, the out-of-plane z component σ_z^v further exemplifies the intertwined nature of the dynamics. When both couplings coexist, we find that the evolution symmetry is broken entirely: σ_z^1 and σ_z^2 evolve in a fashion that is neither symmetric nor antisymmetric [Fig. 4(a)]. Note that, with only

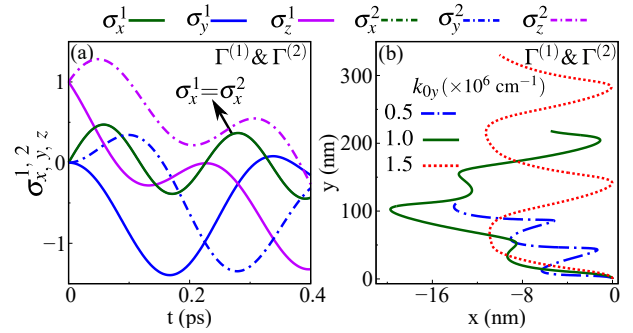


Figure 4. (Color online) (a), (b) Time evolution of the two-band spin components $\sigma_{x,y,z}^v$ (a) and *Zitterbewegung* (b), incorporating both linear ($\Gamma^{(1)}$) and quadratic ($\Gamma^{(2)}$) SO contributions. In (a), $k_{0y} = 0.05 \times 10^6 \text{ cm}^{-1}$; in (b), $k_{0y} = \{0.5, 1.0, 1.5\} \times 10^6 \text{ cm}^{-1}$.

$\Gamma^{(1)}$, the evolution is symmetric ($\sigma_z^1 = \sigma_z^2$), whereas with only $\Gamma^{(2)}$, the dynamics becomes antisymmetric, with σ_z^1 and σ_z^2 evolving in opposite directions from their initial value of 1. As a complement, regarding intertwined effect of $\Gamma^{(1)}$ and $\Gamma^{(2)}$ on spatial *Zitterbewegung*, we find that their coexistence gives rise to combined trembling motions in both the longitudinal and transverse directions [Fig. 4(b); Fig. S4 in the SM].

For completeness, we finally consider the scenario in which both intraband (β_v , $v = 1, 2$) and interband ($\Gamma^{(1)}$; $\Gamma^{(2)}$) terms are present. In the case of “ $\Gamma^{(1)} & \beta_v$ ”, since both $\Gamma^{(1)}$ and β_v are linear in momentum, we find that the symmetric features of spin dynamics are preserved, with $\sigma_z^1 = \sigma_z^2$ and $\sigma_x^1 = \sigma_x^2$ [see the SM; Fig. S6(a)]. In contrast, in the case of “ $\Gamma^{(2)} & \beta_v$ ”, the opposite characteristics between σ_z^1 and σ_z^2 is broken [see the SM; Fig. S6(b)], due to the interplay between the quadratic interband and the linear intraband couplings.

Concluding remarks.— We have uncovered a *quadratic* SO contribution that emerges from interband effects in semiconductor heterostructures, justified by both our model calculations and symmetry analysis along with the method of invariants. We have also found that this unusual *even-order* SO term induces a rich set of spin-related phenomena, including hybridized spin textures, anisotropic dispersions, avoided band crossings, and novel quantum dynamics in both real space and spin space. These intriguing features are not only distinct from those associated with the linear terms, but also highlight new pathways for tailoring spin behavior through interband effects. Our work uncovers a previously overlooked facet of SO physics and points toward novel strategies for spintronic functionalities that leverage interband effect and unusual SO terms of *even* orders, thus holding broad interest from both theoretical and experimental communities. As a final remark, even in the presence of Rashba-type contributions—both intra- and interband—the essential features induced by the quadratic SO term persist (see the SM; Sec. IV), further potentially broadening the frontier of spintronic and even orbitronic functionalities.

Acknowledgments.— This work was supported by the National Natural Science Foundation of China (Grants

No. 12274256, No. 11874236, No. 12022413, No. 11674331, and No. 61674096), the Major Basic Program of Natural Science Foundation of Shandong Province (Grant No. ZR2021ZD01), the National Key R&D Program of China (Grant No. 2022YFA1403200), and the “Strategic Priority Research Program (B)” of the Chinese Academy of Sciences (Grant No. XDB33030100).

* yongjf@qfnu.edu.cn

[1] D. Awschalom, D. Loss, and N. Samarth, *Semiconductor Spintronics and Quantum Computation* (Springer, New York, 2002).

[2] I. Žutić, J. Fabian, and S. D. Sarma, Spintronics: Fundamentals and applications, *Rev. Mod. Phys.* **76**, 323 (2004).

[3] M. Amundsen, J. Linder, J. W. A. Robinson, I. Žutić, and N. Banerjee, Colloquium: Spin-orbit effects in superconducting hybrid structures, *Rev. Mod. Phys.* **96**, 021003 (2024).

[4] J. Fabian, A. Matos-Abiague, C. Ertler, P. Stano, and I. Žutić, Semiconductor Spintronics, *acta physica slovaca* **57**, 565 (2007).

[5] J. Fabian, Spin’s lifetime extended, *Nature* **458**, 580 (2009).

[6] J. R. Bindel, M. Pezzotta, J. Ulrich, M. Liebmann, E. Y. Sherman, and M. Morgenstern, Probing variations of the rashba spin-orbit coupling at the nanometre scale, *Nat. Phys.* **12**, 920 (2016).

[7] E. J. Rodríguez, A. A. Reynoso, J. P. Baltanás, J. Nitta, and D. Frustaglia, Magnetic switching of spin-scattering centers in dresselhaus [110] circuits, *Phys. Rev. B* **109**, 035308 (2024).

[8] J. Nitta, Spin-orbit interaction and spintronics, *JSAP Review* **2023**, 230102 (2023).

[9] Y. A. Bychkov and E. I. Rashba, Properties of a 2D electron gas with lifted spectral degeneracy, *JETP Letters* **39**, 78 (1984).

[10] G. Dresselhaus, Spin-orbit coupling effects in zinc blende structures, *Phys. Rev.* **100**, 580 (1955).

[11] J. D. Koralek, C. P. Weber, J. Orenstein, B. A. Bernevig, S. C. Zhang, S. Mack, and D. D. Awschalom, Emergence of the persistent spin helix in semiconductor quantum wells, *Nature* **458**, 610 (2009).

[12] G. Engels, J. Lange, T. Schäpers, and H. Lüth, Experimental and theoretical approach to spin splitting in modulation-doped $In_xGa_{(1-x)}As/InP$ quantum wells for $b \rightarrow 0$, *Phys. Rev. B* **55**, R1958 (1997).

[13] J. Nitta, T. Akazaki, H. Takayanagi, and T. Enoki, Gate control of spin-orbit interaction in an inverted $In_{0.53}Ga_{0.47}As/In_{0.52}Al_{0.48}As$, *Phys. Rev. Lett.* **78**, 1335 (1997).

[14] F. Dettwiler, J. Y. Fu, S. Mack, P. J. Weigle, J. C. Egues, D. D. Awschalom, and D. M. Zumbühl, Stretchable persistent spin helices in GaAs quantum wells, *Phys. Rev. X* **7**, 031010 (2017).

[15] J. Y. Fu, P. H. Penteado, M. O. Hachiya, D. Loss, and J. C. Egues, Persistent skyrmion lattice of noninteracting electrons with spin-orbit coupling, *Phys. Rev. Lett.* **117**, 226401 (2016).

[16] J. Y. Fu and J. C. Egues, Spin-orbit interaction in GaAs wells: From one to two subbands, *Phys. Rev. B* **91**, 075408 (2015).

[17] M. Studer, M. Walser, S. Baer, H. Rusterholz, S. Schü, D. Schuh, W. Wegscheider, K. Ensslin, and G. Salis, Role of linear and cubic terms for drift-induced Dresselhaus spin-orbit splitting in a two-dimensional electron gas, *Phys. Rev. B* **82**, 235320 (2010).

[18] H. Yang, X. Li, W. Wang, N. Hao, P. Zhang, and J. Y. Fu, Emergence of aligned nontopological and crossed topological spin helices with unconventional spin-orbit manipulation, *Phys. Rev. B* **111**, L241403 (2025).

[19] G. E. Pikus and G. L. Bir, *Symmetry and Strain-Induced Effects in Semiconductors* (Wiley, New York, 1974).

[20] G. Bastard, *Wave Mechanics Applied to Semiconductor Heterostructures* (Halsted, Les Ulis, New York, 1989).

[21] Strictly speaking, the effective 2D mass is given by, $m_{2D}^{*-1} = \langle \nu | m^*(z)^{-1} | \nu \rangle$ [20], making it intrinsically subband (ν) dependent; in Eq. (3), this dependence is neglected for simplicity.

[22] Equation (3) retains SO terms up to the second order in \mathbf{k} , in line with our focus on capturing the quadratic contribution.

[23] D. Varjas, T. Ö. Rosdahl, and A. R. Akhmerov, Qsymm: Algorithmic symmetry finding and symmetric hamiltonian generation, *New J. Phys.* **20**, 093026 (2018).

[24] M. S. Dresselhaus, G. Dresselhaus, and A. Jorio, *Group theory: Application to the physics of condensed matter* (Springer Science & Business Media, 2007).

[25] T. Koga, J. Nitta, T. Akazaki, and H. Takayanagi, Rashba spin-orbit coupling probed by the weak antilocalization analysis in $InAlAs/InGaAs/InAlAs$ quantum wells as a function of quantum well asymmetry, *Phys. Rev. Lett.* **89**, 046801 (2002).

[26] I. Vurgaftman, J. R. Meyer, and L. R. Ram-Mohan, Band parameters for III-V compound semiconductors and their alloys, *J. Appl. Phys.* **89**, 5815 (2001).

[27] Q. X. Wang, H. Yang, and J. Y. Fu, Selective asymmetric gate control of the Rashba spin-orbit coupling in $GaInAs/AlInAs$ stepped wells, *Phys. Rev. B* **101**, 245403 (2020).

[28] F. G. G. Hernandez, L. Nunes, G. Gusev, and A. Bakarov, Observation of the intrinsic spin hall effect in a two-dimensional electron gas, *Phys. Rev. B* **88**, 161305(R) (2013).

[29] R. Song, N. Hao, and P. Zhang, Giant inverse Rashba-Edelstein effect: Application to monolayer $OsBi_2$, *Phys. Rev. B* **104**, 115433 (2021).

[30] G. J. Ferreira, B. Wang, J. Fu, and R. Raimondi, Charge-spin conversion in two-subband quantum wells with conventional and unconventional rashba spin-orbit coupling, in *Spintronics XVI*, Vol. 12656 (SPIE, 2023) pp. 133–153.

[31] H. Bentmann, S. Abdelouahed, M. Mulazzi, J. Henk, and F. Reinert, Direct observation of interband spin-orbit coupling in a two-dimensional electron system, *Phys. Rev. Lett.* **108**, 196801 (2012).

[32] J. Schliemann, D. Loss, and R. Westervelt, Zitterbewegung of electronic wave packets in III-V zinc-blende semiconductor quantum wells, *Phys. Rev. Lett.* **94**, 206801 (2005).

[33] J. Schliemann, D. Loss, and R. Westervelt, Zitterbewegung of electrons and holes in III-V semiconductor quantum wells, *Phys. Rev. B* **73**, 085323 (2006).

[34] W. Zawadzki, Zitterbewegung and its effects on electrons in semiconductors, *Phys. Rev. B* **72**, 085217 (2005).

[35] W. Wen, J. Liang, H. Xu, F. Jin, Y. G. Rubo, T. C. Liew, and R. Su, Trembling motion of exciton polaritons close to the Rashba-Dresselhaus regime, *Phys. Rev. Lett.* **133**, 116903 (2024).

[36] I. Lavor, D. da Costa, L. Covaci, M. Milošević, F. Peeters, and A. Chaves, Zitterbewegung of moiré excitons in twisted MoS_2/WSe_2 heterobilayers, *Phys. Rev. Lett.* **127**, 106801 (2021).

[37] H. Smith, *Introduction to Quantum Mechanics* (World Scientific Publishing Company, 1991).

[38] B. A. Lippmann, Ehrenfest’s theorem and scattering theory, *Phys. Rev. Lett.* **15**, 11 (1965).